*CHEMISTRY JOURNAL OF MOLDOVA. General, Industrial and Ecological Chemistry. 2026, 21(1), 72-85*
*ISSN (p) 1857-1727 ISSN (e) 2345-1688*
*http://cjm.ichem.md*
*https://doi.org/10.19261/cjm.2026.1380*

# INDOLE-BASED SUPPORTED CATALYSTS FOR THE SELECTIVE PHENOL OXIDATION

Savita Kumari [a], Praveen Kumar Gupta [a*], Ram Karan [a], Amit Kumar [b], Ramesh Kumar [c]

[a]*Department of Chemistry, Maharishi Markandeshwar (Deemed to be University), Mullana-133207, Haryana, India*
[b]*Department of Chemistry, Indira Gandhi National College, Ladwa, Kurukshetra-136132, Haryana, India*
[c]*Department of Chemistry, Kurukshetra University, Kurukshetra-136119, Haryana, India*
[*]*e-mail*:*parveen.gupta@mmumullana.org*

**Abstract.** A new class of supported catalysts were synthesized by anchoring 2-((1*H*-indole-3-yl)methyleneamino)phenol (HIMAP) onto chloromethylated polystyrene beads, followed by binding with various metal ions. The catalysts were evaluated for their efficiency in the selective oxidation of phenol under mild conditions using *tert*-butyl hydroperoxides (TBHP) and hydrogen peroxide as oxidants. Among all catalysts, the PS-HIMAP-Cu exhibited superior catalytic performance, achieving up to 97.2% phenol conversion and 91.5% selectivity toward catechol with TBHP. Interestingly, PS-HIMAP-Ni showed the highest catechol selectivity (96.8%) when $H_2O_2$ was employed, despite a lower overall conversion rate. Catalytic efficiency generally peaked at 70°C with 0.15 g of catalyst over 6 hours. Reusability studies demonstrated remarkable stability, with all catalysts retaining high activity over six consecutive cycles, maintaining the structural integrity of the catalysts. Based on elemental, FTIR, EDX, DRS and EPR, the copper catalyst adopts a square-planar geometry, while the nickel and manganese catalysts exhibit tetrahedral coordination environments. The iron catalyst possesses an octahedral geometry, whereas the vanadium catalyst displays a square-pyramidal coordination geometry. The proposed mechanism involves the formation of metal-peroxo intermediates, followed by the electrophilic attack on the phenol ring. This study presents a robust and recyclable catalytic platform of heterogeneous catalysis offering promising avenues for phenol valorisation and wastewater treatment applications.

**Keywords:** polymeric support, functionalized resin, catalysis, reusability, oxidation.

*Received: 22 September 2025/ Revised final: 05 June 2026/ Accepted: 08 June 2026*

## Introduction

The development of polymer-supported metal catalysts has emerged as a promising strategy in modern catalysis, offering a unique combination of the advantages inherent in both homogeneous/heterogeneous catalytic systems. They provide the high selectivity typical of homogeneous catalysts, along with the reusability, ease of separation, and recovery advantages found in heterogeneous approaches [1]. Among various polymeric matrices, chloromethylated polystyrene stands out due to its chemical stability, ease of functionalization, and compatibility with a wide range of ligands and metal ions [2,3]. Schiff base ligands, known for their structural flexibility and strong coordination capability, have played a central role in the design of transition metal complexes for catalytic applications. These ligands, particularly those derived from aromatic aldehydes and amines, have been extensively studied due to their ease of synthesis and ability to stabilize various metal ions in different oxidation states [4]. Schiff base metal complexes have been applied successfully in diverse organic transformations including oxidation, epoxidation, polymerization, *etc*. [5-7]. However, despite their efficacy in homogeneous media, challenges such as catalyst recovery, poor recyclability, and product contamination hinder their practical and industrial application. Immobilising such catalysts on solid supports provides a viable route to overcome these limitations [8,9].

The catalytic oxidation of phenol is a reaction of significant industrial and environmental interest. Catechol and hydroquinone-primary products of phenol oxidation-are key intermediates in the manufacture of pharmaceuticals, agrochemicals and polymers [10,11]. Additionally, phenol is a toxic and unmanageable pollutant commonly found in industrial wastewater, necessitating effective remediation strategies. Heterogeneous catalytic oxidation, especially using supported metal catalysts and green oxidants like hydrogen peroxide and *tert*-butyl

hydroperoxide (TBHP), has been recognised as a sustainable route for phenol degradation and value-added product synthesis [12,13]. Catechol, a major oxidation product, holds immense industrial significance. It serves not only as a precursor for pharmaceuticals and agrochemicals but also widely used in the production of antioxidants, adhesives, and dyes, owing to its strong redox properties [14-17]. Hydroquinone, another oxidation product, finds applications in industrial processes, cosmetics, and medicines. In dermatology, it is frequently used to treat hyperpigmentation conditions by whitening the skin. It acts as an antioxidant in the rubber and polymer industries and stops materials from oxidative degradation [18-20]. Therefore, the design of selective, recyclable, and efficient catalysts for phenol oxidation remains a critical goal.

Several heterogeneous transition metal catalysts have been reported for phenol oxidation using oxidants such as $H_2O_2$ or TBHP. Shen, Y. *et al*. synthesized $Fe^{3+}$ ion-exchanged mesoporous ZSM-5 catalysts, namely Fe-M-ZSM-5 and Fe-ZSM-5/MCM-41, which exhibited 42.3% and 46.2% phenol conversion with 92.5% and 90.1% selectivity toward dihydroxybenzenes, respectively [21]. Castro I.U. *et al*. reported Cu-polymer catalysts for aqueous phenol oxidation, where Cu-PVP afforded nearly 80% phenol conversion under mild conditions (30°C and Ph:$H_2O_2$ molar ratio 1:14) [22]. Maurya, M.R. *et al*. synthesized polymer-supported catalysts PS-[Cu(saldien)] and PS-[VO(saldien)], in which PS-[Cu(saldien)] achieved 22.2% phenol conversion under optimized conditions using $H_2O_2$ at 70°C with *p*-benzoquinone (14.4%) and catechol (7.8%) as major products, whereas PS-[VO(Saldien)] exhibited only 3% conversion with complete selectivity toward benzoquinone in water; however, both catalysts showed enhanced catechol selectivity in acetonitrile medium [23]. Maurya, M.R. *et al*. further developed polystyrene anchored vanadium catalysts, where PS-K[$VO_2$(FSAL-OHYBA)] displayed 37.3% phenol conversion with TOF of 110.5 $h^{-1}$ under optimized conditions (80°C, 6h) and exhibited catechol selectivity of 66.7–69.5% along with 27.5–31.2% hydroquinone formation [24]. In another study, Maurya, M.R. *et al*. investigated zeolite encapsulated [Cu(saldien)]-Y catalyst, which afforded 46.0% phenol conversion with catechol and hydroquinone selectivity of 68.3% and 31.7%, respectively [25]. Bhagya, K.N. *et al*. reported [Cu(2-MeImzlH)]-Y catalyst showing significantly higher phenol conversion (72.5%), although with comparatively lower catechol selectivity (58.8%) [26]. In contrast, Abbo, H.S. *et al*. synthesized $CuL_2(H_2O)_2$-Y catalyst that exhibited lower conversion (18.0%) but exceptionally high catechol selectivity (94.6%), indicating strong ortho-hydroxylation preference [27]. Maurya, M.R. *et al*. also reported [Cu(sal-ambmz)Cl]-Y catalyst with moderate catalytic activity, achieving 42.0% conversion and 73.9% catechol selectivity using $H_2O_2$ as oxidant [28]. Biernacka, I. *et al*. employed Cu(salen)-Y zeolite catalyst using TBHP oxidant and obtained 46.0% phenol conversion with remarkably high catechol selectivity (99.0%) after 48 h reaction time [29]. Shilpa, E.R. *et al*. synthesized Cu(opbmzl)$_2$-Y catalyst, which demonstrated superior catalytic efficiency under optimized conditions (80°C, 6 h), achieving 86.7% phenol conversion with product selectivity toward catechol (66.8%), hydroquinone (18.9%) and benzoquinone (14.3%) [30]. Furthermore, Shakiyeva, T.V. *et al*. reported $CoFe_2O_4$/PVP magnetic composite catalyst for phenol oxidation using $H_2O_2$, where more than 95% phenol conversion was achieved after 2 h with hydroquinone (28%) and benzoquinone (50%) as the major oxidation products [31].

Indole-derived Schiff base ligands have gained considerable importance because of their diverse biological, coordination and catalytic properties. In particular, indole-3-carboxaldehyde based Schiff bases are widely utilized as valuable intermediates for the synthesis of several biologically and chemically important compounds [32]. Indole-3-carboxaldhyde and its derivatives are not only the key intermediates for the preparation of biologically active molecules as well indole alkaloids, but also they are important precursors for the synthesis of diverse heterocyclic derivatives [33]. Owing to the presence of donor sites and extended conjugation, their metal complexes have been investigated for various applications including antimicrobial activity, antibiotic adsorbent materials and catalytic oxidation reactions [34,35].

The novelty of the present work lies in the development of a new series of indole-based metal catalysts. Unlike previously reported catalytic systems, an important feature of the present study is the synthesis of a series of catalysts containing different metal ions including Cu(II), Ni(II), Fe(III), Mn(II) and V(IV), which provides a platform to directly compare the catalytic activity, selectivity and oxidation behaviour of different

transition metals using the same ligand framework and substrate under similar reaction conditions. The obtained catalytic performance is superior to many previously reported polymer-supported and zeolite-encapsulated transition metal catalysts for phenol oxidation, demonstrating the enhanced efficiency and selectivity of the present catalytic system. The catalysts also showed excellent structural stability and recyclability over six consecutive catalytic cycles without significant loss of activity, highlighting their practical applicability in sustainable oxidation processes. This approach aims to establish a sustainable, efficient, and recyclable catalytic platform for industrially significant oxidation reactions.

## Experimental

### *Material and methods*

All chemicals used in the experiment were of analytical grade and employed without purification. 2-Aminophenol and indole-3-carboxaldehyde were procured from Sigma-Aldrich and used for the synthesis of ligand. Metal salts including iron(III) chloride hexahydrate, copper(II) chloride pentahydrate, nickel(II) chloride hexahydrate, manganese(II) acetate tetrahydrate, and vanadyl sulphate were obtained from Central Drug House (P) Ltd (CDH). Phenol, hydrogen peroxide (30% w/w), *tert*-butyl hydroperoxide (70% w/w), and solvents such as acetonitrile, methanol, ethanol, and acetone were also purchased from CDH and used as received. Chloromethylated polystyrene resin was supplied as a gift sample by Thermax Limited, Pune, India. The ligand 2-((1*H*-indole-3-yl) methyleneamino)phenol was synthesized using the reported procedure[36].

The structural and compositional features of the synthesized compounds were elucidated using analytical techniques. FT-IR spectra were recorded in the range 400-4000 $cm^{-1}$ using a Shimadzu IR Spirit spectrophotometer to confirm functional group transformations and metal coordination. Diffuse reflectance spectroscopy (DRS) was carried out on a Shimadzu UV-2600 double beam spectrophotometer using $BaSO_4$ as the reference standard to assess electronic transitions and geometry. Elemental analysis (CHNS) was performed with a Thermo Scientific Flash 2000 analyser to determine the elemental composition of the supported ligand and catalysts. The metal loading on the supported catalysts was quantified using atomic absorption spectroscopy (AAS) on a Shimadzu ASC-6880 instrument. EDX (Energy-dispersive X-ray) spectra were obtained through a Hitachi SU8010 Series FEG scanning electron microscope to confirm the presence of metal ions. ESR (Electron spin resonance) spectra of Cu(II), V(IV), and Mn(II) complexes were measured at room temperature using a JES FA200 spectrometer to probe the oxidation states and coordination environment of the metal centres. Additionally, GC-MS analysis was conducted on an Agilent 7000 GC/TQ system to monitor the phenol oxidation products and confirm their identity.

### *Immobilization of 2-((1H-Indole-3-yl) methyleneamino)phenol on chloromethylated polystyrene*

A quantity of 3.5 g of resin was first swollen in 30 mL of DMF for 1 hour to enhance its reactivity. Separately, 3.7 g (15.75 mmol) of the pre-synthesized Schiff base ligand, 2-((1*H*-indole-3-yl)methyleneamino)phenol (HIMAP), was dissolved in DMF (20 mL) and added dropwise to the swollen resin under stirring. To facilitate nucleophilic substitution, 3.2 mL of triethylamine was added, and the reaction mixture was heated at 80°C for 8 hours. During the course of the reaction, the colour of the resin gradually changed to a deep brown, indicating successful ligand attachment. The functionalized beads were then cooled to room temperature, filtered and thoroughly washed with hot DMF and ethanol to remove any unreacted species. Finally, the resulting immobilized ligand (PS-HIMAP) was dried at 80°C.

### *Synthesis of metal-loaded PS-HIMAP catalysts*

The functionalized beads (PS-HIMAP) (4.5–9.0 mmol) was pre-swollen in 20 mL of DMF for 1 h to ensure proper diffusion and interaction during complexation. Separately, 4.5 mmol of the respective metal salt: $VOSO_4 \cdot 5H_2O$, $CuCl_2 \cdot 2H_2O$, $Mn(CH_3COO)_2 \cdot 4H_2O$, $NiCl_2 \cdot 6H_2O$, or $FeCl_3 \cdot 6H_2O$ was dissolved in DMF and gradually added to the pre-swelled polymer suspension under continuous stirring. As the reaction progressed, a visible change in the colour of the resin indicated successful coordination of the metal ions. The reaction mixture was heated under reflux for 8–12 hours and then allowed to cool to room temperature. The resulting metal bound resin was filtered, washed thoroughly with hot ethanol, methanol and acetone to remove unbound species, and finally dried at 80°C.

### *Catalytic activity study*

Phenol oxidation supported catalysts were carried out in a thermostatted two-neck round bottom flask. The catalysts (0.1–0.15 g) were pre-swollen in 20 mL of acetonitrile for 30 minutes, followed by the addition of phenol (10 mmol) and an oxidant (10 mmol) such as

*t*-BuOOH or $H_2O_2$. The reaction was conducted at 70°C under stirring for varying durations (3–6 h). Progress was monitored *via* TLC, and product identification was confirmed by GC-MS. A blank run without catalyst was also performed for comparison. After completion, the catalyst was recovered by filtration, washed, vacuum-dried, and reused.

## Results and discussion

Polymer beads were successfully functionalized with 2-((1*H*-indole-3-yl) methyleneamino)phenol (HIMAP), yielding the immobilized ligand PS-HIMAP, as depicted in Scheme 1. A noticeable colour change in the resin beads during the reaction confirmed ligand attachment, which was further supported by a negative chlorine test. Subsequent binding with metal resulted in the formation of supported metal catalysts (Scheme 2), also evidenced by distinct colour changes. During the synthesis, 4.5 mmol/g of the respective metal salts, were used for complex formation with PS-HIMAP. The ligand loading values obtained for the polymer-supported ligand and metal complexes were found to lie in the range of 1.74–2.53 mmol/g, whereas the metal loading values after complex formation were observed in the range 0.99–1.52 mmol/g (Table 1). The formation of both the ligand and metal catalysts were finally confirmed through characterization techniques, and representative images are shown in Figure S1 of Supplementary material.

### *Characterization*

### *NMR analysis*

The $^1$H NMR spectrum of 2-((1*H*-indole-3-yl)methyleneamino)phenol confirms the successful formation of the Schiff base ligand as shown in Figure S 2 (see Supplementary material). A singlet observed at $\delta$ 10.07 ppm is assigned to the indole N–H proton. The azomethine proton (–CH=N–) appears as a singlet at $\delta$ 8.80 ppm, confirming the formation of the Schiff base linkage. The phenolic –OH proton resonates as a singlet at $\delta$ 8.33 ppm due to hydrogen bonding effects. Multiplet signals appearing in the aromatic region between $\delta$ 7.29–8.31 ppm are attributed to the aromatic protons of the indole and phenyl rings. The observed chemical shifts are in good agreement with the proposed structure of the ligand.

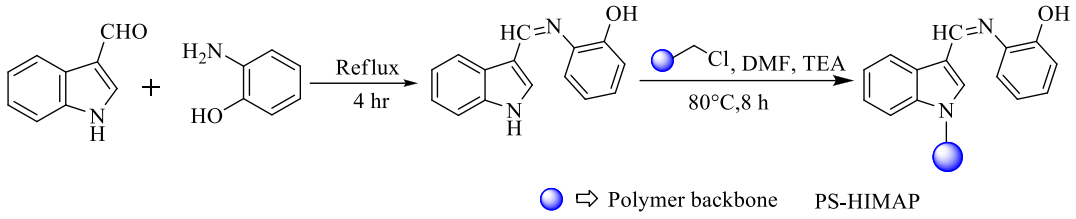


**Scheme 1**. **Preparation of polystyrene anchored ligand**.

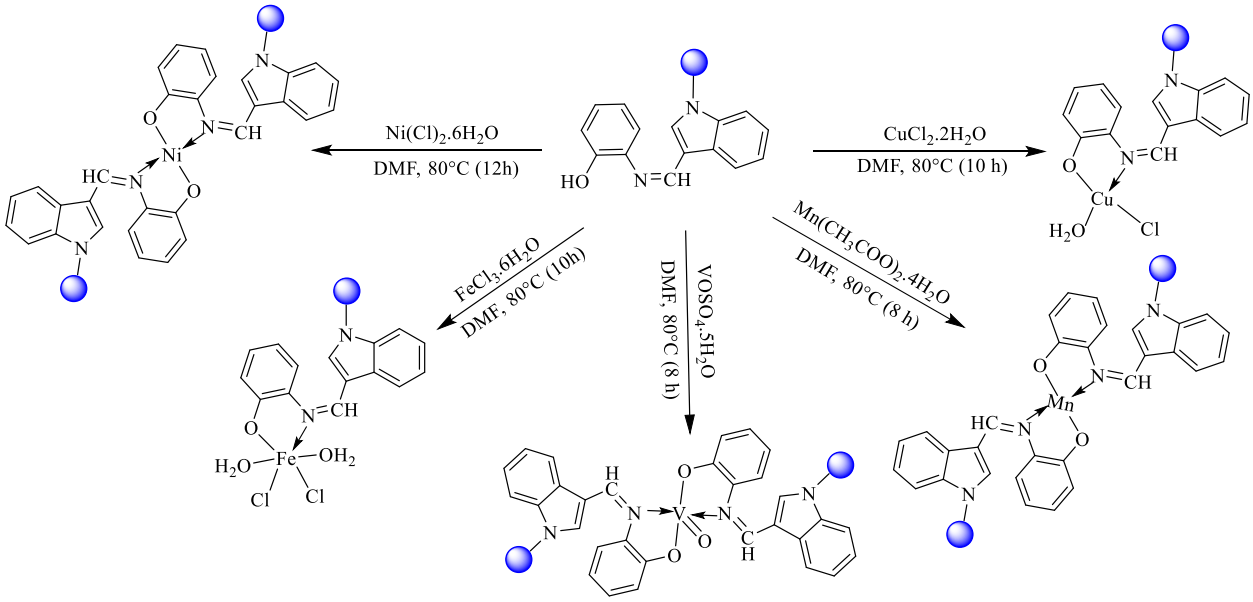


**Scheme 2. Preparation of polystyrene anchored metal catalysts.**

***Elemental analysis***

The successful immobilization of the Schiff base ligand onto the polystyrene matrix and subsequent coordination with transition metal ions were confirmed through elemental analysis. Metal incorporation was further verified by atomic absorption spectroscopy, which quantified the metal content in the supported catalysts, as summarized in Table 1.

***EDX analysis***

Figure S3 (see Supplementary material) shows the EDX spectra of the supported catalysts, confirming the presence of metal ions in all samples. Notably, the spectra of copper and iron complexes also exhibit chlorine signals, indicating the involvement of chloride ions in metal coordination.

***SEM analysis***

The surface morphology of the PS-HIMAP and its corresponding metal catalysts was examined by SEM analysis (Figure S4, see Supplementary material). The SEM micrograph of the PS-HIMAP reveals a comparatively smooth and homogeneous surface morphology. However, after binding with metal ions, changes in the surface texture were observed, with the metal-loaded catalysts exhibiting rough and irregular surface features. Such morphological alterations indicate successful incorporation of the metal species onto the functionalized polymer. Moreover, the catalyst images show uniform dispersion of the metal particles throughout the polymer surface, suggesting effective immobilization and good distribution of the catalytically active sites over the support matrix.

***FTIR spectra***

FTIR spectroscopy was used to verify both the successful loading of the ligand onto the polymer resin and the subsequent coordination of metal ions, as shown in Figure S5 (see Supplementary material) and summarized in Table 2. The characteristic C=N stretching band at 1644 $cm^{-1}$ in PS-HIMAP shifts to a lower wavenumber upon metal coordination, indicative of the participation of azomethine nitrogen in bonding [36]. The broad band at 3368 $cm^{-1}$ confirms the presence of -OH groups in the ligand [38]. This band disappears upon metal coordination, while a new band emerges in the range of 1240–1245 $cm^{-1}$, which can be attributed to the C–O stretching vibration in the metal catalyst. Additional bands observed in the regions 454–473 $cm^{-1}$ and 553–577 $cm^{-1}$ are attributed to M-N and M-O bonds, respectively [39]. Vanadium complexes specifically show a band near 982 $cm^{-1}$ due to $\upsilon$(V=O) stretching [40], while absorption bands between 3392−3405 $cm^{-1}$ confirm the coordination of water molecules [41].

***Diffused reflectance spectra***

Reflectance spectral studies, presented in Figure S6 (see Supplementary material) and Table 3, were employed to investigate the electronic structures of the solid, insoluble supported catalysts. The spectrum of the free ligand [PS-HIMAP] displayed intraligand absorption bands at 37878 and 32258 $cm^{-1}$, corresponding to $\pi \rightarrow \pi^*$ and $n \rightarrow \pi^*$ transitions, respectively. Upon metal coordination, these bands shifted and new d–d transitions appeared, indicating successful complex formation.

*Table 1*

**Analytical data of immobilized resin and its catalysts.**

| *Immobilized resin/ catalysts* | *Colour* | *Elemental analysis %* | | | | *Ligand binding (mmol per gram of resin)* | *Metal binding (mmol per gram of resin)* | *Ligand : Metal Binding* |
|---|---|---|---|---|---|---|---|---|
| | | *C* | *H* | *N* | *M* | | | |
| **[PS-HIMAP]** | Light brown | 82.81 | 6.71 | 7.11 | - | 2.53 | - | - |
| **[PS-HIMAP-Cu]** | Yellow | 65.82 | 5.12 | 4.87 | 8.5 | 1.74 | 1.35 | 1.28:1 |
| **[PS-HIMAP-Mn]** | Yellowish gold | 78.51 | 6.64 | 6.02 | 5.09 | 2.15 | 1.06 | 2.02:1 |
| **[PS-HIMAP-V]** | Olive green | 77.71 | 6.23 | 6.52 | 4.92 | 2.33 | 1.17 | 1.99:1 |
| **[PS-HIMAP-Ni]** | Brown | 78.32 | 6.52 | 5.62 | 5.85 | 2.01 | 0.99 | 2.03:1 |
| **[PS-HIMAP-Fe]** | Dark brown | 63.29 | 5.70 | 4.31 | 8.53 | 1.54 | 1.52 | 1.01:1 |

*Table 2*

**FTIR data for the PS-HIMAP and its metal catalyst.**

| *Compounds* | *υ(C=N)* | *υ(OH)/υ(C-O)* | *υ($H_2O$)* | *υ(V=O)* | *υ(M-O)* | *υ(M-N)* | *υ(M-Cl)* |
|---|---|---|---|---|---|---|---|
| **[PS-HIMAP]** | 1644 | 3368 | - | - | - | - | - |
| **[PS-HIMAP-Cu]** | 1620 | 1245 | 3404 | - | 553 | 467 | 352 |
| **[PS-HIMAP-Ni]** | 1619 | 1245 | - | - | 540 | 460 | 354 |
| **[PS-HIMAP-Fe]** | 1631 | 1242 | 3392 | - | 560 | 467 | 355 |
| **[PS-HIMAP-Mn]** | 1625 | 1240 | - | - | 528 | 473 | - |
| **[PS-HIMAP-V]** | 1632 | 1240 | - | 982 | 577 | 454 | - |

For [PS-HIMAP-Cu], d–d bands at 11764, 16339, 2471 $cm^{-1}$ were observed, corresponding to $^2B_{1g} \rightarrow {}^2A_{1g}$, $^2B_{1g} \rightarrow {}^2B_{2g}$, $^2B_{1g} \rightarrow {}^2E_g$ transitions, suggesting a square planar geometry [42]. The [PS-HIMAP-Ni] complex exhibited spin-allowed transitions at 10775, 16366, and 24038 $cm^{-1}$ due to $^3A_2 \rightarrow {}^3T_2(G)(\nu_1)$, $^3A_2 \rightarrow {}^3T_1(F)(\nu_2)$, and $^3A_2 \rightarrow {}^3T_1(P)(\nu_3)$, consistent with a tetrahedral Ni(II) environment [43]. [PS-HIMAP-Fe] showed bands at 12165, 16501, and 21505 $cm^{-1}$, attributed to $^6A_{1g} \rightarrow {}^4T_{1g}(G)(\nu_1)$, $^6A_{1g} \rightarrow {}^4T_{2g}(F)$ $(\nu_2)$ and $^6A_{1g} \rightarrow {}^4T_{1g}(P)$ $(\nu_3)$ transitions, respectively [44]. For [PS-HIMAP-Mn], two bands at 16000 and 23753 $cm^{-1}$ indicated $^6A_1 \rightarrow {}^4T_1(G)$ and $^6A_1 \rightarrow {}^4T_2(G)$ transitions, also supporting a tetrahedral geometry [45]. The vanadium complex [PS-HIMAP-V] exhibited transitions at 12345, 16103, and 22883 $cm^{-1}$, corresponding to $^2B_{2g} \rightarrow {}^2E_g$; $^2B_{2g} \rightarrow {}^2B_{1g}$ and $^2B_{2g} \rightarrow {}^2A_{1g}$, typical of five-coordinate oxovanadium(IV) species [46].

***EPR studies***

Figure 1 presents the room-temperature EPR spectra of the supported Cu(II), Mn(II) and V(IV) catalysts. The EPR spectra were recorded for polymer-supported catalysts in powder form with an estimated uncertainty of approximately ±0.002 for g-values and ±5 × $10^{-4}$ $cm^{-1}$ for hyperfine coupling constants. Owing to the heterogeneous and amorphous nature of the polymer matrix, line broadening and partial overlap of spectral features are commonly observed.

*Table 3*

**DRS spectral data of polystyrene-anchored metal complexes.**

| *Supported catalysts* | *d→d band position in $cm^{-1}$* | *d→d band assignment* |
|---|---|---|
| **[PS-HIMAP-Cu]** | 11764, 16339, 24271 | $^2B_{1g} \rightarrow {}^2A_{1g}$, $^2B_{1g} \rightarrow {}^2B_{2g}$, $^2B_{1g} \rightarrow {}^2E_g$ |
| **[PS-HIMAP-Ni]** | 10775, 16366, 24038 | $^3A_2 \rightarrow {}^3T_2(G)$, $^3A_2 \rightarrow {}^3T_1(F)$, $^3A_2 \rightarrow {}^3T_1(P)$ |
| **[PS-HIMAP-Fe]** | 12165, 12406, 21505 | $^6A_{1g} \rightarrow {}^4T_{1g}(G)(\nu_1)$, $^6A_{1g} \rightarrow {}^4T_{2g}(F)$, $^6A_{1g} \rightarrow {}^4T_{1g}(P)$ |
| **[PS-HIMAP-Mn]** | 16000, 21505 | $^6A_1 \rightarrow {}^4T_1(G)$, $^6A_1 \rightarrow {}^4T_2(G)$ |
| **[PS-HIMAP-V]** | 12345, 16103, 22883 | $^2B_{2g} \rightarrow {}^2E_g$, $^2B_{2g} \rightarrow {}^2B_{1g}$, $^2B_{2g} \rightarrow {}^2A_{1g}$ |

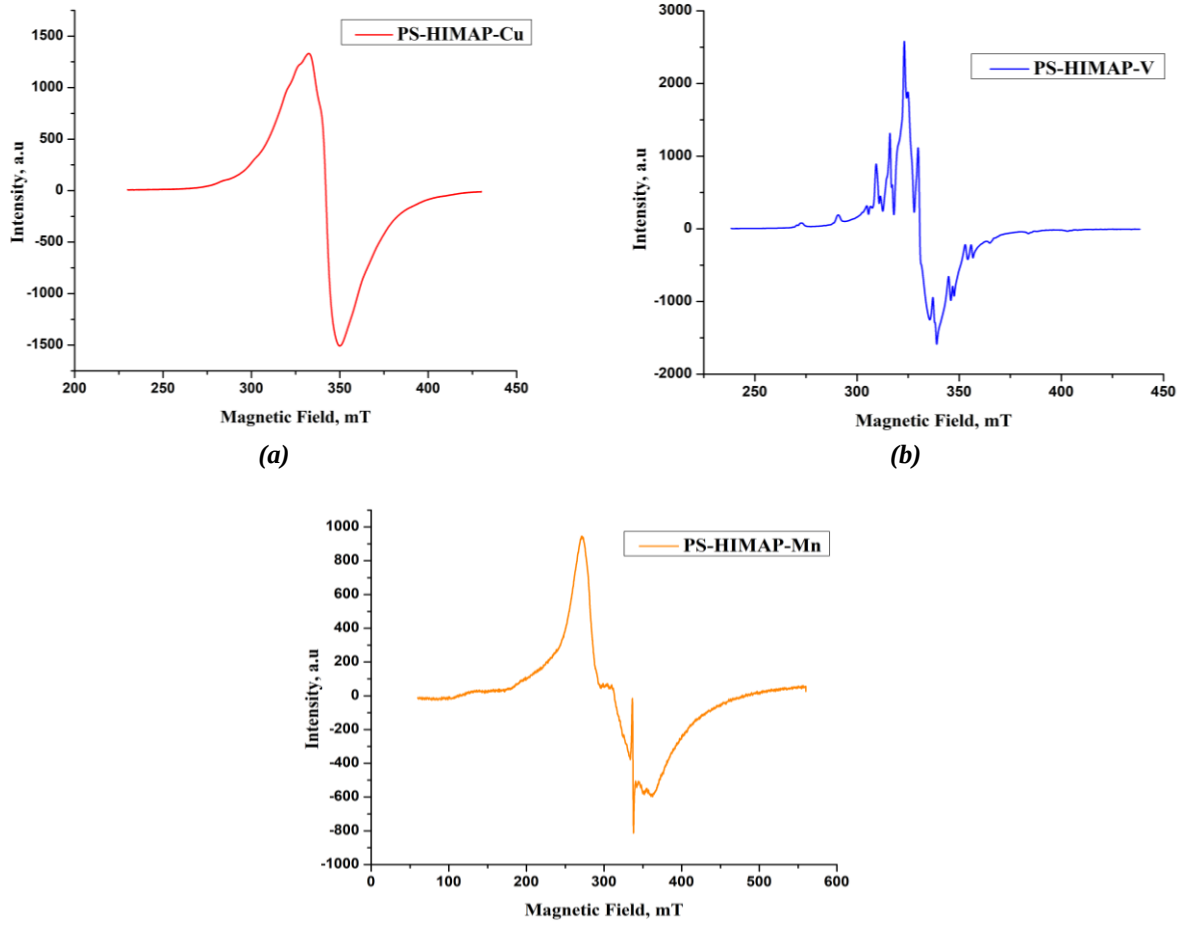


***(a)*** ***(b)*** ***(c)***

**Figure 1. EPR spectra of [PS-HIMAP-Cu]** ***(a)*****, [PS-HIMAP-V]** ***(b)*** **and [PS-HIMAP-Mn]** ***(c)*****.**

Consequently, the anisotropic components are not always fully resolved for Cu(II), Mn(II) and V(IV) systems. The reported g and A parameters were therefore obtained from the average positions of the observable resonance and hyperfine features of the powder spectra. The [PS-HIMAP-V] spectrum displays an axially symmetric signal, characteristic of V(IV) species. The hyperfine splitting into eight lines in both perpendicular and parallel regions confirm the presence of isolated V(IV) centres with no V-V interactions. The observed anisotropic parameters ($A_\perp$= 74 G; $A_\parallel$= 185 G; $g_\perp$= 2.04 and $g_\parallel$= 1.99) ($A_\perp < A_\parallel$; $g_\perp > g_\parallel$) are consistent with a square pyramidal geometry and $C_{4v}$ symmetry, with the V=O bond aligned along the z-axis [47]. The Mn(II) catalyst [PS-HIMAP-Mn] exhibits six hyperfine lines due to the coupling of unpaired electron and nuclear spin. The spectral features and Hamiltonian parameters [g= 2.15 and A= 144 G] support a tetrahedral geometry around Mn(II) centres [48]. For the [PS-HIMAP-Cu] catalyst, an axial spectrum is observed with $g_\parallel > g_e$ ($g_\parallel$= 2.15) and four hyperfine lines in the parallel region with an average separation of 177 G, indicates a square planar environment [49].

The geometries for Cu(II), Mn(II) and V(IV) complexes have been assigned based on above explained characterization data [ligand-to-metal binding ratios, FTIR spectral shifts and metal-ligand vibration bands, EDX, d-d transition bands obtained from DRS studies and the EPR spectral parameters]. Accordingly, [PS-HIMAP-Cu] was assigned a square-planar geometry based on characteristic d-d transitions and axial EPR spectrum. [PS-HIMAP-Ni] and [PS-HIMAP-Mn] were assigned tetrahedral geometry from their electronic spectral transitions. [PS-HIMAP-Fe] showed spectral transitions consistent with an octahedral geometry. [PS-HIMAP-V] exhibited characteristic oxovanadium(IV) transitions and EPR parameters corresponding to square-pyramidal geometry.

***Catalytic activity***

Supported catalysts were evaluated for their catalytic performance in phenol oxidation at 70°C using $H_2O_2$ and TBHP as oxidants. The study examined the influence of catalyst loading, reaction temperature, and reaction time on the reaction outcome. The oxidation of phenol in acetonitrile at 70°C using TBHP and $H_2O_2$ produced catechol and hydroquinone as the major product. Various reaction parameters were systematically optimised to determine the conditions that maximize catalytic activity and product selectivity. The corresponding results are summarized in Tables 4 and 5.

***Effect of temperature***

The conversion of phenol gets enhanced as the reaction temperature rise from 60°C to 70°C; however, further rise beyond 70°C did not result in any significant improvement in phenol oxidation.

***Effect of catalyst amount***

The effect of catalyst loading on phenol oxidation was investigated by varying the catalyst amount from 0.1 to 0.15 g, while maintaining a constant 1:2 molar ratio of substrate to oxidant. An increase in catalyst amount led to higher phenol conversion up to 0.15 g. However, further increase beyond this point showed no significant enhancement in conversion, indicating an optimal catalyst loading threshold.

*Table 4*

**Conversion of phenol and product selectivity.**

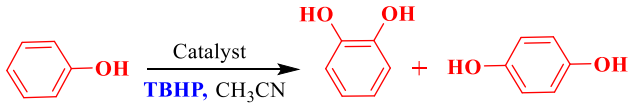


| *Compound* | *Catalyst concentration (g)* | *Time (h)* | *% Conversion* | *% Selectivity* | | |
|---|---|---|---|---|---|---|
| | | | | *CTL* | *HQ* | *Others* |
| **Blank** | | 3 | 4.6 | 62.2 | 10.1 | 27.7 |
| | | 4 | 6.2 | 62.6 | 10.3 | 27.1 |
| | | 5 | 6.8 | 63.1 | 10.3 | 26.6 |
| | | 6 | 9.1 | 63.3 | 10.4 | 26.3 |
| **PS-HIMAP-Cu** | 0.1 | 3 | 83.5 | 89.5 | 9.5 | 1.0 |
| | | 4 | 87.1 | 89.5 | 9.7 | 0.8 |
| | | 5 | 92.7 | 90,1 | 9.6 | 0.3 |
| | | 6 | 94.2 | 91.1 | 8.7 | 0.2 |
| | 0.15 | 3 | 88.2 | 89.8 | 9.6 | 0.6 |
| | | 4 | 90.3 | 90.2 | 9.4 | 0.4 |
| | | 5 | 95.1 | 90.9 | 8.9 | 0.2 |
| | | 6 | 97.2 | 91.5 | 8.1 | 0.4 |

*Continuation of Table 4*

| *Compound* | *Catalyst concentration (g)* | *Time (h)* | *% Conversion* | *% Selectivity* | | |
|---|---|---|---|---|---|---|
| | | | | *CTL* | *HQ* | *Others* |
| **PS-HIMAP-Ni** | 0.1 | 3 | 59.2 | *CTL* | *HQ* | *Others* |
| | | 4 | 61.1 | 71.1 | 28.1 | 0.8 |
| | | 5 | 65.3 | 71.2 | 27.9 | 0.9 |
| | | 6 | 67.9 | 73.5 | 25.8 | 0.7 |
| | 0.15 | 3 | 62.8 | 72.3 | 26.5 | 1.2 |
| | | 4 | 65.2 | 77.4 | 22.1 | 0.5 |
| | | 5 | 69.5 | 77.8 | 21.7 | 0.5 |
| | | 6 | 73.1 | 78.9 | 20.6 | 0.5 |
| **PS-HIMAP-Fe** | 0.1 | 3 | 80.1 | 80.5 | 19.3 | 0.2 |
| | | 4 | 83.4 | 81.1 | 18.2 | 0.7 |
| | | 5 | 87.7 | 82.7 | 17.2 | 0.1 |
| | | 6 | 91.1 | 82.8 | 16.8 | 0.4 |
| | 0.15 | 3 | 83.1 | 82.3 | 17.6 | 0.1 |
| | | 4 | 86.3 | 83.5 | 16.3 | 0.2 |
| | | 5 | 90.2 | 85.9 | 13.7 | 0.4 |
| | | 6 | 93.8 | 86.1 | 13.4 | 0.5 |
| **PS-HIMAP-Mn** | 0.1 | 3 | 49.3 | 69.2 | 29.8 | 1.0 |
| | | 4 | 51.1 | 69.4 | 30.1 | 0.5 |
| | | 5 | 53.5 | 70.2 | 28.9 | 0.9 |
| | | 6 | 55.9 | 71.1 | 28.3 | 0.6 |
| | 0.15 | 3 | 50.1 | 70.2 | 28.5 | 1.3 |
| | | 4 | 53.2 | 71.5 | 28.1 | 0.4 |
| | | 5 | 53.9 | 72.2 | 26.9 | 0.9 |
| | | 6 | 56.6 | 73.7 | 25.7 | 0.6 |
| **PS-HIMAP-V** | 0.1 | 3 | 54.8 | 60.1 | 38.8 | 1.1 |
| | | 4 | 56.1 | 60.1 | 38.7 | 1.2 |
| | | 5 | 58.7 | 62.2 | 37.1 | 0.7 |
| | | 6 | 61.8 | 63.7 | 36.1 | 0.2 |
| | 0.15 | 3 | 57.7 | 62.1 | 37.3 | 0.6 |
| | | 4 | 59.1 | 63.5 | 36.2 | 0.3 |
| | | 5 | 62.2 | 66.4 | 33.1 | 0.5 |
| | | 6 | 66.8 | 67.9 | 31.8 | 0.3 |

CTL = Catechol, HQ = Hydroquinone; *Reaction setup: 20 ml of $CH_3CN$, 10 mmol of Phenol, 20 mmol of TBHP, temperature: 70°C.

*Table 5*

**Conversion of phenol and product selectivity.**

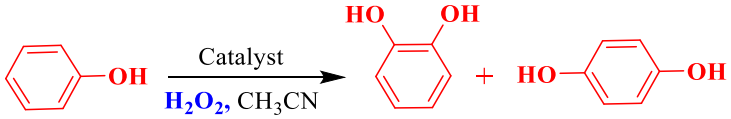


| *Compound* | *Catalyst concentration (g)* | *Time (h)* | *% Conversion* | *% Selectivity* | | |
|---|---|---|---|---|---|---|
| | | | | *CTL* | *HQ* | *Others* |
| **Blank** | | 3 | 4.1 | 56.7 | 9.6 | 33.7 |
| | | 4 | 5.8 | 56.8 | 9.7 | 33.5 |
| | | 5 | 6.2 | 56.8 | 9.9 | 33.3 |
| | | 6 | 8.8 | 56.9 | 10.1 | 33.0 |
| **PS-HIMAP-Cu** | 0.1 | 3 | 80.1 | 68.3 | 30.9 | 0.8 |
| | | 4 | 82.5 | 68.4 | 30.8 | 0.8 |
| | | 5 | 88.7 | 69.5 | 29.7 | 0.8 |
| | | 6 | 92.3 | 70.1 | 29.4 | 0.5 |
| | 0.15 | 3 | 85.1 | 69.1 | 29.9 | 1.0 |
| | | 4 | 85.3 | 69.5 | 29.8 | 0.7 |
| | | 5 | 90.6 | 70.2 | 29.5 | 0.3 |
| | | 6 | 92.9 | 70.9 | 28.8 | 0.3 |

*Continuation of Table 5*

| *Compound* | *Catalyst concentration (g)* | *Time (h)* | *% Conversion* | *% Selectivity* | | |
|---|---|---|---|---|---|---|
| | | | | *CTL* | *HQ* | *Others* |
| **PS-HIMAP-Ni** | 0.1 | 3 | 57.1 | *CTL* | *HQ* | *Others* |
| | | 4 | 59.2 | 92.1 | 6.9 | 1.0 |
| | | 5 | 61.5 | 93.3 | 6.2 | 0.5 |
| | | 6 | 64.2 | 93.5 | 6.1 | 0.4 |
| | 0.15 | 3 | 58.7 | 95.3 | 3.4 | 1.3 |
| | | 4 | 62.4 | 95.5 | 3.8 | 0.5 |
| | | 5 | 63.5 | 96.6 | 2.7 | 0.5 |
| | | 6 | 67.1 | 96.8 | 2.1 | 0.8 |
| **PS-HIMAP-Fe** | 0.1 | 3 | 76.5 | 75.6 | 24.1 | 0.3 |
| | | 4 | 78.4 | 76.2 | 23.3 | 0.5 |
| | | 5 | 80.3 | 76.5 | 23.2 | 0.3 |
| | | 6 | 83.5 | 77.9 | 21.9 | 0.2 |
| | 0.15 | 3 | 78.3 | 75.9 | 23.7 | 0.4 |
| | | 4 | 80.2 | 76.7 | 23.1 | 0.2 |
| | | 5 | 83.1 | 77.2 | 22.4 | 0.4 |
| | | 6 | 85.8 | 78.4 | 20.9 | 0.2 |
| **PS-HIMAP-Mn** | 0.1 | 3 | 47.1 | 64.1 | 34.5 | 1.4 |
| | | 4 | 48.3 | 65.4 | 33.9 | 0.7 |
| | | 5 | 49.5 | 65.5 | 34.4 | 0.1 |
| | | 6 | 52.7 | 67.7 | 31.9 | 0.4 |
| | 0.15 | 3 | 48.2 | 64.7 | 34.8 | 0.5 |
| | | 4 | 49.2 | 65.9 | 34.5 | 0.4 |
| | | 5 | 51.1 | 68.5 | 30.2 | 1.2 |
| | | 6 | 52.9 | 70.3 | 29.3 | 0.4 |
| **PS-HIMAP-V** | 0.1 | 3 | 52.2 | 55.9 | 43.9 | 0.2 |
| | | 4 | 53.1 | 56.2 | 42.8 | 1.2 |
| | | 5 | 55.9 | 56.6 | 43.1 | 0.3 |
| | | 6 | 59.2 | 58.7 | 40.2 | 1.1 |
| | 0.15 | 3 | 53.4 | 56.1 | 42.6 | 1.3 |
| | | 4 | 54.2 | 56.9 | 42.9 | 0.2 |
| | | 5 | 57.6 | 57.8 | 42.1 | 0.1 |
| | | 6 | 61.7 | 60.3 | 39.5 | 0.2 |

* Reaction setup: 20 ml of $CH_3CN$, 10 mmol of Phenol, 20 mmol of $H_2O_2$, temperature: 70°C.

***Effect of oxidant***

The influence of two oxidants, $H_2O_2$ and TBHP, on the catalytic performance of the supported catalysts in phenol oxidation was evaluated. As shown in Tables 4 and 5, TBHP provided the highest conversion rate of 97.2% with the Cu(II) catalyst, while $H_2O_2$ yielded the maximum catechol selectivity of 96.8% with the Ni(II) catalyst.

***Effect of time***

The progress of the reaction was examined by performing phenol oxidation using 1:2 ratio of TBHP/$H_2O_2$, and 0.1 g/0.15 g of catalyst at an ideal temperature of 70°C with continuous stirring. Minimal reaction progress was observed in the first 2 hours, indicating an initiation phase of the reaction. After that, for all catalysts, phenol conversion rise gradually as reaction durations increased. The maximum conversion rate was attained at 6 hours, as seen in Figure S7 (see Supplementary material), when results from 3 to 8 hours were compared. Furthermore, when reaction time increased, the selectivity for various compounds was generally constant.

***Recyclability test***

Reusability tests showed that the supported catalyst retained nearly constant catalytic activity for up to six cycles before a marked decline was observed (Figure 2 and Table S8 in Supplementary material). This reduction in efficiency may be attributed to catalyst decomposition in the reaction medium or leaching into the organic solvent during product isolation. Notably, catechol selectivity remained unchanged with the recycled catalyst, suggesting that the metal complex maintained its structural integrity on the polymer support, which was further supported by the comparing the spectra of fresh and recycled catalysts.

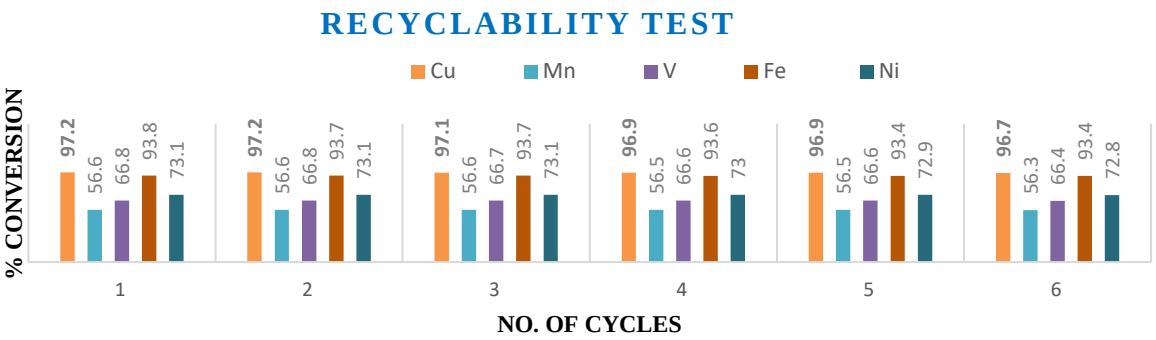


**Figure 2. Recyclability test of supported catalysts.**

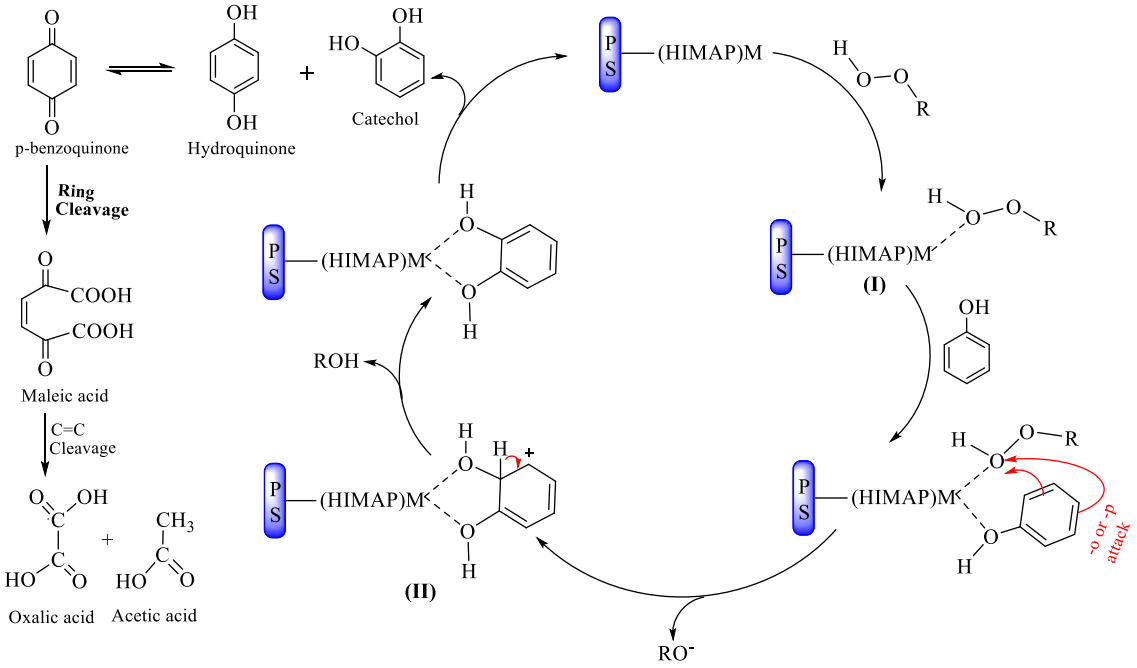


**Scheme 3. Proposed pathway for $H_2O_2$/TBHP-assisted phenol oxidation catalysed by the supported system.**

*Table 6*

**Metal leaching analysis of polymer-anchored catalysts.**

| *No.of cycle* | *Cu (%)* | *Fe (%)* | *Ni (%)* | *V (%)* | *Mn (%)* |
|---|---|---|---|---|---|
| **1st** | 0.02 | 0.03 | 0.05 | 0.07 | 0.1 |
| **2nd** | 0.03 | 0.05 | 0.07 | 0.08 | 0.13 |
| **3rd** | 0.04 | 0.06 | 0.09 | 0.09 | 0.14 |
| **4th** | 0.06 | 0.08 | 0.1 | 0.12 | 0.16 |
| **5th** | 0.08 | 0.09 | 0.12 | 0.15 | 0.17 |
| **6th** | 0.09 | 0.12 | 0.13 | 0.17 | 0.17 |
| **7th** | 3.52 | 3.71 | 3.71 | 3.98 | 4.10 |

### *Metal leaching quantification*

The metal leaching remained negligible (<0.18 %) up to the sixth catalytic cycle, confirming strong metal-ligand interaction and catalyst stability (Table 6). However, a significant increase in leaching (3.52–4.10%) was observed in the seventh cycle, which correlates with the decrease in catalytic activity. The delayed onset of metal leaching demonstrates that the catalyst possesses high structural integrity and stability for multiple cycles before gradual deactivation occurs.

### *Plausible mechanism for oxidation of phenol*

$H_2O_2$ or TBHP interacts with the metal centre forming a peroxo-metal complex (I). Thereafter, phenol also coordinates to the metal catalyst. The O–O bond in the oxidant is polarised and activated for transfer of one oxygen atom to the *ortho*/*para* position of the phenol ring *via* a concerted transition state. This forms a hydroxycyclohexadienone-type intermediate (II), which undergo electron reorganisation, leading to the formation of catechol (if *ortho* attack) or hydroquinone (if *para* attack) (Scheme 3).

*Table 7*

**Comparative study with unsupported complexes.**

| *Unsupported metal complexes* | *Reaction Condition Oxidant/Solvent/Temp/Time* | *% Conversion* | *% Selectivity, Catechol* | *Ref.* |
|---|---|---|---|---|
| 3MHBdMBn-Met complexes [Met = Fe(III), Co(II), Ni(II), Cu(II) and Zn(II) ions] | $H_2O_2$ / $CH_3CN$ / 70°C / 24 h | 50.5% | 96.5% | [50] |
| N,N-bis(o-hydroxyacetophenone) hydrazine (HPHZ) Schiff base Fe(III), Co(II) and Ni(II) catalyst | $H_2O_2$ / $CH_3CN$ / 70°C / 24 h | 56.0% | 86% | [51] |
| $MnL^1{}_2Cl$ and $MnL^2{}_2Cl$; M = Mn(III); $L^1$ = *N*,*N*′-bis(salicylidene)-o-phenylene diamine Schiff base ligand; $L^2$ = *N*,*N*′-bis(salicylidene)-2,2-dimethyl-1,3-propanediamine Schiff base ligand | $H_2O_2$ / pH 7.0 phosphate buffer / 35°C / 8 h | - | - | [52] |
| VO-(EtOsalphen)[3-ethoxy salicylaldehyde-1,2 -diaminobenzene]; VO-(EtOsalnaph) [3-ethoxy salicylaldehyde-1,8-diaminonaphthalene] | $H_2O_2$ / $CH_3CN$ / 70°C / 6 h | 71.0%<br>76.6% | 92.5%<br>94.2% | [53] |
| Cu(II)/2,6-dihydroxypyridine | $H_2O_2$ / $H_2O$ / 65°C / 30 min | 23.0% | 89.0% | [54] |
| $[Ni\{Me_4Bzo_2[14]aneN_4\}]Cl_2$ | $H_2O_2$ / $H_2O$ / 80°C / 360 min | 15.0% | 85.0% | [55] |
| PS-HIMAP-Cu [Polymer-supported Cu(II) complex of 2-((1H-indole-3-yl) methyleneamino)phenol] | TBHP / $CH_3CN$ / 70°C / 6 h | 97.2% | 91.5% | Present work |

The other oxidation products formed during the reaction include *o*-benzoquinone, *p*-benzoquinone, maleic acid, oxalic acid and acetic acid. The oxidation of catechol and hydroquinone leads to the formation of *o*-benzoquinone and *p*-benzoquinone, respectively. Under oxidative conditions, these quinone intermediates undergo oxidative ring cleavage producing low molecular weight acids such as maleic acid, which upon further oxidative cleavage, forms oxalic acid and acetic acid as final degradation products. During the catalytic cycle, the active metal centre is regenerated by release of water or *tert*-butanol (confirmed in GC-MS), depending upon the oxidant employed, thereby completing the catalytic oxidation pathway (Scheme 3).

***Comparative study with the unsupported metal catalyst***

To further evaluate the efficiency of the synthesised polymer-supported metal catalysts, the catalytic performance of the present system was compared with previously reported unsupported transition metal catalysts employed for phenol oxidation. The comparative data summarised in Table 7 demonstrate that the present PS-HIMAP-Cu catalyst exhibits better catalytic activity in terms of phenol conversion and catechol selectivity under relatively mild reaction conditions. The enhanced catalytic performance may be attributed to the polymer support, effective immobilisation of the active metal centre and the presence of the indole-based Schiff base framework.

**Conclusions**

In this study, a new series of polymer supported metal catalysts were developed by loading the ligand 2-((1*H*-indole-3-yl)methyleneamino) phenol (HIMAP) onto chloromethylated polystyrene, followed by binding with various transition metal ions. Spectroscopic and analytical techniques confirmed the successful immobilization of the ligand and subsequent metal coordination, with each catalyst exhibiting distinct structural and electronic features. The catalytic activity of these materials was systematically evaluated for the selective oxidation of phenol using oxidants (TBHP and $H_2O_2$) under mild conditions. Catalytic parameters including temperature, catalyst loading, oxidant type, and reaction time were optimized, revealing that 70°C, 0.15 g catalyst loading, and 6 hours reaction time constituted the optimal conditions. With TBHP, the phenol conversion efficiency followed the sequence: PS-HIMAP-Cu > PS-HIMAP-Fe > PS-HIMAP-Ni > PS-HIMAP-V > PS-HIMAP-Mn, whereas catechol selectivity decreased in the order: PS-HIMAP-Cu > PS-HIMAP-Fe > PS-HIMAP-Ni > PS-HIMAP-Mn > PS-HIMAP-V. In contrast, for $H_2O_2$ mediated oxidation, the conversion trend remained similar, while catechol selectivity was observed in the order: PS-HIMAP-Ni > PS-HIMAP-Fe > PS-HIMAP-Cu > PS-HIMAP-Mn > PS-HIMAP-V. Among the synthesised catalysts, PS-HIMAP-Cu emerged as the most efficient, achieving a maximum conversion of 97.2% and catechol selectivity of 91.5% with TBHP. Conversely, PS-HIMAP-Ni demonstrated superior

selectivity for catechol (96.8%) when $H_2O_2$ was used as the oxidant, despite lower conversion, highlighting the role of both metal centre and oxidant in tuning product selectivity. Other metal catalysts such as PS-HIMAP-Fe, PS-HIMAP-Mn, and PS-HIMAP-V also showed notable activity, with Fe showing high conversion and V showing the least activity under the studied conditions. All catalysts exhibited excellent recyclability and retained structural integrity over six consecutive cycles, confirming their robustness and potential for practical applications.

## Supplementary information

Supplementary data are available free of charge at http://cjm.ichem.md as PDF file.

## References


1. Madhavan, N.; Jones, C.W.; Weck, M. Rational approach to polymer-supported catalysts: synergy between catalytic reaction mechanism and polymer design. Accounts of Chemical Research, 2008, 41(9), pp. 1153–1165. DOI: https://doi.org/10.1021/ar800081y
2. Altava, B.; Burguete, M.I.; García-Verdugo, E.; Luis, S.V. Chiral catalysts immobilized on achiral polymers: effect of the polymer support on the performance of the catalyst. Chemical Society Reviews, 2018, 47(8), pp. 2722–2771. DOI: https://doi.org/10.1039/C7CS00734E
3. Mohammadi, E.; Movassagh, B. Synthesis of polystyrene-supported Pd(II)-NHC complex derived from theophylline as an efficient and reusable heterogeneous catalyst for the Heck-Matsuda cross-coupling reaction. Journal of Molecular Catalysis A: Chemical, 2016, 418–419, pp. 158–167. DOI: https://doi.org/10.1016/j.molcata.2016.03.045
4. Gupta, K.C.; Sutar, A.K. Catalytic activities of Schiff base transition metal complexes. Coordination Chemistry Reviews, 2008, 252(12-14), pp. 1420–1450. DOI: https://doi.org/10.1016/j.ccr.2007.09.005
5. Santoro, O.; Zhang, X.; Redshaw, C. Synthesis of biodegradable polymers: a review on the use of Schiff-base metal complexes as catalysts for the ring opening polymerization (ROP) of cyclic esters. Catalysts, 2020, 10(7), 800, pp. 1–48. DOI: https://doi.org/10.3390/catal10070800
6. Zoubi, W.A.; Ko, Y.G. Schiff base complexes and their versatile applications as catalysts in oxidation of organic compounds: part I. Applied Organometallic Chemistry, 2017, 31(3), e3574. DOI: https://doi.org/10.1002/aoc.3574
7. Visuvamithiran, P.; Palanichamy, M.; Shanthi, K.; Murugesan, V. Selective epoxidation of olefins over Co(II)-Schiff base immobilised on KIT-6. Applied Catalysis A: General, 2013, 462–463, pp. 31–38. DOI: https://doi.org/10.1016/j.apcata.2013.05.007
8. Kumari, S.; Gupta, P.K.; Rawal, R.K.; Kumar, S. Reusable metal bound polystyrene-anchored thiophene-2-carboxaldehyde catalysts for efficient oxidation of benzyl alcohol. Russian Journal of General Chemistry, 2024, 94, pp. 3401–3412. DOI: https://doi.org/10.1134/S1070363224120326
9. Kumari, S.; Kumar, S.; Karan, R.; Bhatia, R.; Kumar, A.; Rawal, R.K.; Gupta, P.K. Synthetic and catalytic perspectives of polystyrene supported metal catalyst. Journal of Iranian Chemical Society, 2024, 21(4), pp. 951–1010. DOI: https://doi.org/10.1007/s13738-024-02970-7
10. Gamez, P.; Schütz, J.; Netscher, T. Phenol oxidations. Stahl, S.S.; Alsters, P.L. Eds. Liquid phase aerobic oxidation catalysis: industrial applications and academic perspectives. Wiley-VCH: Weinheim, 2016, pp. 97–111. DOI: https://doi.org/10.1002/9783527690121.ch7
11. Naranov, E.; Ramazanov, D.; Agliullin, M.; Sinyashin, O.; Maximov, A. Recent advances in aromatic hydroxylation to phenol and hydroquinone using $H_2O_2$. Catalysts, 2024, 14(12), 930, pp. 1–23. DOI: https://doi.org/10.3390/catal14120930
12. Srikhaow, A.; Smith, S.M.; Uraisin, K.; Suttiponparnit, K.; Kongmark, C.; Chuaicham, C. Catalytic remediation of phenol contaminated wastewater using Cu–Zn hydroxide nitrate. RSC Advances, 2016, 6(43), pp. 36766–36774. DOI: https://doi.org/10.1039/C5RA22326A
13. Zamisa, M.K.; Seadira, T.W.; Baloyi, S.J. Transforming wastewater treatment: recent advancements in catalytic wet air oxidation with pillared clay catalysts for phenol remediation. Environmental Pollution, 2024, 361, 124842, pp. 1–22. DOI: https://doi.org/10.1016/j.envpol.2024.124842
14. Belmekki, B.; Terkhi, M.C.; Messai, R.; Ferhat, M.F.; Ghezzar, M.R. A novel approach of catechol production assisted by plasma process: Lab-scale experiment and modeling, commercial-scale design and economic evaluation. Chemical Engineering Journal, 2024, 502, 157844, pp. 1–15. DOI: https://doi.org/10.1016/j.cej.2024.157844
15. Zhao, K.; Wang, B.; Zhang, C.; Guo, Y.; Ma, Y.; Li, Z.; Wu, T.; Bao, Z.; Gao, Y.; Du, F. Catechol functionalized hat-shape carriers for prolonging pesticide retention and flush resistance on foliage. Chemical Engineering Journal, 2021, 420(2), 127689, pp. 1–11. DOI: https://doi.org/10.1016/j.cej.2020.127689
16. Su, J.; Chen, F.; Cryns, V.L.; Messersmith, P.B. Catechol polymers for pH-responsive, targeted drug delivery to cancer cells. Journal of the American Chemical Society, 2011, 133(31), pp. 11850–11853. DOI: https://doi.org/10.1021/ja203077x
17. Faure, E.; Falentin-Daudré, C.; Jérôme, C.; Lyskawa, J.; Fournier, D.; Woisel, P.; Detrembleur, C. Catechols as versatile platforms in polymer chemistry. Progress in Polymer Science, 2013, 38(1), pp. 236–270. DOI: https://doi.org/10.1016/j.progpolymsci.2012.06.004
18. Fabian, I.M.; Sinnathamby, E.S.; Flanagan, C.J.; Lindberg, A.; Tynes, B.; Kelkar, R.A.; Varrassi, G.; Ahmadzadeh, S.; Shekoohi, S.; Kaye, A.D. Topical hydroquinone for hyperpigmentation: A narrative review. Cureus, 2023, 15(11), e48840, pp. 1–5. DOI: https://doi.org/10.7759/cureus.48840
19. Enguita, F.J.; Leitão, A.L. Hydroquinone: environmental pollution, toxicity, and microbial answers. BioMed Research International, 2013, (1), 542168, pp. 1–14. DOI: https://doi.org/10.1155/2013/542168

20. Liu, F.; Liu, Y.; Dong, H.; Shao, H.; Su, B.; Zhou, T.; Guan, X. Sulfate radicals-mediated chemiluminescence production with peroxydisulfate and hydroquinone as coreactants: mechanism and environmental applications. ACS ES&T Engineering, 2024, 4(9), pp. 2234–2242. DOI: https://doi.org/10.1021/acsestengg.4c00219
21. Shen, Y.; Wang, F.; Liu, W.; Zhang, X. The preparation of $Fe^{3+}$ ion-exchanged mesopore containing ZSM-5 molecular sieves and its high catalytic activity in the hydroxylation of phenol. Journal of Porous Materials, 2018, 25, pp. 1587–1595. DOI: https://doi.org/10.1007/s10934-018-0572-9
22. Castro, I.U.; Stüber, F.; Fabregat, A.; Font, J.; Fortuny, A.; Bengoa, C. Supported Cu(II) polymer catalysts for aqueous phenol oxidation. Journal of Hazardous Materials, 2009, 163(2-3), pp. 809–815. DOI: https://doi.org/10.1016/j.jhazmat.2008.07.054
23. Maurya, M.R.; Sikarwar, S. Oxidation of phenol and hydroquinone catalysed by copper(II) and oxovanadium(IV) complexes of *N*,*N*′-bis(salicyledene)diethylenetriamine ($H_2$saldien) covalently bonded to chloromethylated polystyrene. Journal of Molecular Catalysis A: Chemical, 2007, 263(1-2), pp. 175–185. DOI: https://doi.org/10.1016/j.molcata.2006.08.038
24. Maurya, M.R.; Kumar, U.; Manikandan, P. Polymer supported vanadium and molybdenum complexes as potential catalysts for the oxidation and oxidative bromination of organic substrates. Dalton Transactions, 2006, (29), pp. 3561–3575. DOI: https://doi.org/10.1039/B600822D
25. Maurya, M.R.; Titinchi, S.J.J.; Chand, S. Oxidation of phenol with $H_2O_2$catalysed by Cu(II), Ni(II) and Zn(II) complexes of *N*,*N*-bis-(salicylidene)diethylenetriamine ($H_2$saldien) encapsulated in Y-zeolite. Journal of Molecular Catalysis A: Chemical, 2003, 201(1-2), pp. 119–130. DOI: https://doi.org/10.1016/S1381-1169(03)00193-6
26. Bhagya, K.N.; Gayathri, V. Metal complexes of 2-methylimidazole encapsulated in zeolite-Y as efficient and reusable catalysts for oxidation of phenol and benzyl alcohol. Journal of Porous Materials, 2013, 20, pp. 257–266. DOI: https://doi.org/10.1007/s10934-012-9595-9
27. Abbo, H.S.; Titinchi, S.J.J. Synthesis and catalytic activity of Cu(II), Fe(III) and Bi (III) complexes of thio-Schiff base encapsulated in zeolite-Y for hydroxylation of phenol. Topics in Catalysis, 2010, 53, pp. 254–264. DOI: https://doi.org/10.1007/s11244-009-9408-9
28. Maurya, M.R.; Chandrakar, A.K.; Chand, S. Oxidation of phenol, styrene and methyl phenyl sulfide with $H_2O_2$ catalysed by dioxovanadium(V) and copper(II) complexes of 2-aminomethylbenzimidazole-based ligand encapsulated in zeolite-Y. Journal of Molecular Catalysis A: Chemical, 2007, 263(1-2), pp. 227–237. DOI: https://doi.org/10.1016/j.molcata.2006.08.084
29. Kuźniarska-Biernacka, I.; Carvalho, M.A.; Rasmussen, S.B.; Bañares, M.A.; Biernacki, K.; Magalhães, A.L.; Rolo, A.G.; Fonseca, A.M.; Neves, I.C. Copper(II)–imida-salen complexes encapsulated into NaY zeolite for oxidations reactions. European Journal of Inorganic Chemistry, 2013, 31, pp. 5408–5417. DOI: https://doi.org/10.1002/ejic.201300656
30. Shilpa, E.R.; Gayathri, V. Encapsulation of Cu(II)[2-(2′-hydroxyphenyl)benzimidazole]$_2$ within zeolite nano-cavity: Structural properties and its catalytic activity towards phenol and styrene oxidation. Journal of Environmental Chemical Engineering, 2016, 4(4A), pp. 4194–4206. DOI: https://doi.org/10.1016/j.jece.2016.09.022
31. Shakiyeva, T.V.; Dossumova, B.T.; Sassykova, L.R.; Ilmuratova, M.S.; Dzhatkambayeva, U.N.; Abildin, T.S. Study of the oxidation of phenol in the presence of a magnetic composite catalyst $CoFe_2O_4$/Polyvinylpyrrolidone. Applied Sciences, 2024, 14(19), 8907, pp. 1–23. DOI: https://doi.org/10.3390/app14198907
32. El-Sawy, E.R.; Abo-Salem, H.M.; Mandour, A.H. 1H-Indole-3-carboxaldehyde: Synthesis and Reactions. Egyptian Journal of Chemistry, 2017, 60(5), pp. 723–751. DOI: https://doi.org/10.21608/EJCHEM.2017.1097.1053
33. Priya, B.; Utreja, D.; Kalia, A. Schiff bases of indole-3-carbaldehyde: Synthesis and evaluation as antimicrobial agents. Russian Journal of Bioorganic Chemistry, 2022, 48, pp. 1282–1290. DOI: https://doi.org/10.1134/S1068162022060188
34. Reshma, R.; Joseyphus, R.S.; Dasan, A.; John, L. Synthesis and spectral characterization of metal complexes of Schiff base derived from indole-3-carboxaldehyde and L-histidine as potent biocides. Journal of Coordination Chemistry, 2019, 72(19-21), pp. 3326–3337. DOI: https://doi.org/10.1080/00958972.2019.1695126
35. Moghaddam-Manesh, M.M.; Darvishi, R.; Barati, A.; Moshkriz, A.; Seyedsharifi, M. Synthesis of novel $Fe_3O_4$@gly@Indole@$CuNO_3$ magnetic nanoparticle as high-performance antibiotic absorbent, antimicrobial agent, and reusable magnetic Nano catalyst. Journal of Environmental Chemical Engineering, 2025, 13(1), 114970, pp. 1–18. DOI: https://doi.org/10.1016/j.jece.2024.114970
36. Sinha, D.; Tiwari, A.K.; Singh, S.; Shukla, G.; Mishra, P.; Chandra, H.; Mishra, A.K. Synthesis, characterization and biological activity of Schiff base analogues of indole-3-carboxaldehyde. European Journal of Medicinal Chemistry, 2008, 43(1), pp. 160–165. DOI: https://doi.org/10.1016/j.ejmech.2007.03.022
Chandra, S.; Jain, D.; Sharma, A.K.; Sharma, P. Coordination modes of a Schiff base pentadentate derivative of 4-aminoantipyrine with cobalt(II), nickel(II) and copper(II) metal ions: synthesis, spectroscopic and antimicrobial studies. Molecules, 2009, 14(1), pp. 174–190. DOI: https://doi.org/10.3390/molecules14010174
37. Mohamed, M.; Abdelakder, H.; Abdellah, B. Microwave assisted synthesis of 4-aminophenol Schiff bases: DFT computations, QSAR/Drug-likeness proprieties and antibacterial screening. Journal of Molecular Structure, 2021, 1241, 130666, pp. 1–15. DOI: https://doi.org/10.1016/j.molstruc.2021.130666
38. Siddappa, K.; Mane, S.B.; Manikprabhu, D. Spectral characterization and 3D molecular modeling studies of metal complexes involving the O,N-donor environment of quinazoline-4(3H)-one schiff base and their biological studies. The Scientific World Journal, 2014, (1), 817365, pp. 1–13.

DOI: https://doi.org/10.1155/2014/817365
39. Papanikolaou, M.; Hadjithoma, S.; Keramidas, O.; Drouza, C.; Amoiridis, A.; Themistokleous, A.; Hayes, S.C.; Miras, H.N.; Lianos, P.; Tsipis, A.C.; Kabanos, T.A.; Keramidas, A.D. Experimental and theoretical investigation of the mechanism of the reduction of $O_2$ from air to $O_2^{2-}$ by $V^{IV}O^{2+}$–N,N,N-amidate compounds and their potential use in fuel cells. Inorganic Chemistry, 2024, 63(7), pp. 3229–3249.
DOI: https://doi.org/10.1021/acs.inorgchem.3c03272
40. Abd El-Halim, H.; El-Sayed, O.Y.; Mohamed, G.G. Anti-carcinoma and anti-microbial behavioral studies for octahedral synthesized Schiff base metal complexes. Journal of the Iranian Chemical Society, 2023, 20, pp. 2713–2725.
DOI: https://doi.org/10.1007/s13738-023-02868-w
41. Dick, A.; Rahemi, H.; Krausz, E.R.; Hanson, G.R.; Riley, M.J. The highly resolved electronic spectrum of the square planar $CuCl_4^{2-}$ ion. The Journal of Chemical Physics, 2008, 129(21), 214505, pp. 1–8.
DOI: https://doi.org/10.1063/1.3033367
42. Joseyphus, R.S.; Nair, M.S. Synthesis, characterization and biological studies of some Co(II), Ni(II) and Cu(II) complexes derived from indole-3-carboxaldehyde and glycylglycine as Schiff base ligand. Arabian Journal of Chemistry, 2010, 3(4), pp. 195–204.
DOI: http://doi.org/10.1016/j.arabjc.2010.05.001
43. Sohtun, W.P.; Khamrang, T.; Kannan, A.; Balakrishnan, G.; Saravanan, D.; Akhbarsha, M.A.; Velusamy, M.; Palaniandavar, M. Iron(III) bis-complexes of Schiff bases of S-methyldithiocarbazates: Synthesis, structure, spectral and redox properties and cytotoxicity. Applied Organometallic Chemistry, 2020, 34(5), e5593, pp. 1–14.
DOI: https://doi.org/10.1002/aoc.5593
44. Morad, V.; Cherniukh, I.; Pöttschacher, L.; Shynkarenko, Y.; Yakunin, S.; Kovalenko, M.V. Manganese(II) in tetrahedral halide environment: factors governing bright green luminescence. Chemistry of Materials, 2019, 31(24), pp. 10161–10169.
DOI: https://doi.org/10.1021/acs.chemmater.9b03782
45. Kumar, R.; Singh, P.; Kumar, U.; Singh, S.S.; Saha, A.K.; Sharma, S. Spectroscopic characterization of some oxovanadium(IV, V) complexes. Asian Journal of Chemistry, 2014, 26(16), pp. 5298–5300.
DOI: http://doi.org/10.14233/ajchem.2014.17755
46. Borah, R.; Lahkar, S.; Deori, N.; Brahma, S. Synthesis, characterization and application of oxovanadium(IV) complexes with [NNO] donor ligands: X-ray structures of their corresponding dioxovanadium(V) complexes. RSC Advances, 2022, 12(22), pp. 13740–13748.
DOI: https://doi.org/10.1039/D2RA01448C
47. Chandra, S.; Gupta, L.K. EPR, IR and electronic spectral studies on Mn(II), Co(II), Ni(II) and Cu(II) complexes with a new 22-membered azamacrocyclic $[N_4]$ ligand. Spectrochimica Acta Part A: Molecular and Biomolecular Spectroscopy, 2004, 60(8-9), pp. 1751–1761.
DOI: https://doi.org/10.1016/j.saa.2003.07.011
48. Oladipo, S.D.; Luckay, R.C. Copper(II) complexes derived from naphthalene-based halogenated Schiff bases: Synthesis, structural analysis, DFT computational studies and *in vitro* biological activities. New Journal of Chemistry, 2024, 48(30), pp. 13276–13288.
DOI: https://doi.org/10.1039/D4NJ01621A
49. Nath, N.; Routaray, A.; Das, Y.; Maharana, T.; Sutar, A.K. Synthesis and structural studies of polymer-supported transition metal complexes: Efficient catalysts for oxidation of phenol. Kinetics and Catalysis, 2015, 56(6), pp. 718–732.
DOI: https://doi.org/10.1134/S0023158415060105
50. Gupta, K.C; Sutar, A.K. Polymer supported Schiff base complexes of iron(III), cobalt(II) and nickel(II) ions and their catalytic activity in oxidation of phenol and cyclohexene. Journal of Macromolecular Science, Part A: Pure and Applied Chemistry, 2007, 44(11), pp. 1171–1185.
DOI: https://doi.org/10.1080/10601320701561106
51. Zhang, J.; Tang, Y.; Xie, J.-Q.; Li, J.-Z.; Zeng, W.; Hu, C.-W. Study on phenol oxidation with $H_2O_2$ catalyzed by Schiff base manganese complexes as mimetic peroxidise. Journal of Serbian Chemical Society, 2005, 70(10), pp. 1137–1146.
DOI: https://doi.org/10.2298/JSC0510137Z
52. Alsalim, T.A.; Hadi, J.S.; Al-Nasir, E.A.; Abbo, H.S.; Titinchi, S.J.J. Hydroxylation of phenol catalyzed by oxovanadium(iv) of salen-type Schiff base complexes with hydrogen peroxide. Catalysis Letters, (2010), 136(3-4), pp. 228–233.
DOI: https://doi.org/10.1007/s10562-010-0326-z
53. Karakhanov, E.A.; Maximov, A.L.; Kardasheva, Y.S.; Skorkin, V.A.; Kardashev, S.V.; Ivanova, E.A.; Lurie-Luke, E.; Seeley, J.A.; Cron, S.L. Hydroxylation of phenol by hydrogen peroxide catalyzed by copper(II) and iron(III) complexes: the structure of the ligand and the selectivity of ortho-hydroxylation. Industrial & Engineering Chemistry Research, 2010, 49(10), pp. 4607–4613.
DOI: https://doi.org/10.1021/ie902040m
54. Abbob, H.S.; Titinchi, S.J.J.; Chand, S.; Prasad, R. Investigation of $[Ni\{Me_4Bzo_2[14]aneN_4\}]Cl_2$ catalyzed selective hydroxylation of phenol to catechol by $H_2O_2$ in the homogeneous medium. Journal of Molecular Catalysis A: Chemical, 2004, 218(2), pp. 125–132.
DOI: https://doi.org/10.1016/j.molcata.2004.04.012